Optimal deformable mirror and pupil apodization combinations for apodized pupil Lyot coronagraphs with obstructed pupils

Kevin Fogarty, Johan Mazoyer, Kathryn St. Laurent, Rémi Soummer, Mamadou N'Diaye, et al.

Kevin Fogarty, Johan Mazoyer, Kathryn St. Laurent, Rémi Soummer, Mamadou N'Diaye, Chris Stark, Laurent Pueyo, "Optimal deformable mirror and pupil apodization combinations for apodized pupil Lyot coronagraphs with obstructed pupils," Proc. SPIE 10698, Space Telescopes and Instrumentation 2018: Optical, Infrared, and Millimeter Wave, 106981J (21 August 2018); doi: 10.1117/12.2314394

SPIE.

Event: SPIE Astronomical Telescopes + Instrumentation, 2018, Austin, Texas, United States

Optimal Deformable Mirror and Pupil Apodization Combinations for Apodized Pupil Lyot Coronagraphs with Obstructed Pupils

Kevin Fogarty[a], Johan Mazoyer[b], Kathryn St. Laurent[a], Rémi Soummer[a], Mamadou N'Diaye[c], Chris Stark[a], Laurent Pueyo[a]

[a] Space Telescope Science Institute, 3700 San Martin Drive, Baltimore, MD 21218, USA
[b] Johns Hopkins University Department of Physics and Astronomy, 3800 San Martin Drive, Baltimore, MD 21218, USA
[c] Université Cote d´Azur, Observatoir de la Cote d´Azur, CNRS, Laboratoire Lagrange, F-06108 Nice, France

ABSTRACT

Combining active pupil correction via deformable mirrors (DMs) with coronagraphs such as the Apodized Pupil Lyot Coronagraph (APLC) provides a powerful tool for creating high contrast dark holes with obstructed pupils featuring central obstructions, spiders, and gaps. We investigate optimal combinations of DM pupil remapping via Active Compensation of Aperture Discontinuities- Optimized Stroke Minimization (ACAD-OSM) and binary mask pupil apodization to obtain dark holes with contrasts of 10^{10} for the APLC. We examine the space of possible configurations for an APLC apodized with a circularly symmetric pupil mask and a pair of DMs using a modified MCMC algorithm that allows us to probe previously unexamined combinations of pupil apodization, focal plane mask size, and Lyot stop size. We find designs with $\sim 20\%$ encircled energy throughput for a focal plane mask radius of $4.5\lambda/D$ and a bandwidth of 20%, as well as for a focal plane mask radius of 3.18 λ/D and a bandwidth of 10%. We also find solutions for focal plane mask radii of ~ 2 λ/D and 20% bandwidths that can obtain encircled energy throughputs of up to $\sim 4\%$. Our strategy of combining circularly symmetric binary masks with DMs to create dark holes with obstructed pupils can be expanded to optimize the APLC for terrestrial exoplanet yield, and we conclude by exploring the possibility of optimizing coronagraphs using a simple parametric expression for yield.

Keywords: apodized pupil Lyot coronagraph, APLC, deformable mirrors, ACAD-OSM, exoplanet, high-contrast imaging, yield, SCDA

1. INTRODUCTION

High contrast imaging using coronagraphs on space telescopes will allow us to detect and spectroscopically characterize terrestrial exoplanets, paving the way for either finding or placing upper limits on the incidence of biosignatures on planets outside the solar system.[1–3] Recently, several missions have been proposed that would facilitate this endeavor, such as LUVOIR and Habex.[2,4] These missions will need to fly either one or a combination of the coronagraphs that have been developed to obtain the $\sim 10^{10}$ contrast ratio necessary to observe terrestrial exoplanets in optical light, such as the Apodized Pupil Lyot Coronagraph (APLC), the Vector Vortex Coronagraph, or the Phase-Induced Amplitude Apodization (PIAA) coronagraph.[5–15]

Coronagraphs designed for future space telescopes need to compensate for obstructed telescope pupils, which feature segment gaps, and in the case of an on-axis secondary mirror, spiders and a central obstruction. Recently, it was shown that APLCs with binary pupil masks can correct for pupil obstructions and create image-plane dark holes with contrasts of 10^{10}.[16,17] While previous results have demonstrated how an APLC can obtain a broadband dark hole with 10^{10} contrast with smoothly varying apodizers,[6] being able to use binary pupil masks

Further author information, send correspondence to Kevin Fogarty: E-mail: kfogarty@stsci.edu

Space Telescopes and Instrumentation 2018: Optical, Infrared, and Millimeter Wave, edited by Makenzie Lystrup, Howard A. MacEwen, Giovanni G. Fazio, Proc. of SPIE Vol. 10698, 106981J
 · doi: 10.1117/12.2314394

(which allow transmission to be either 1 or 0 across the pupil plane) increases the feasibility of the APLC, since binary apodizers can be produced with achromatic transmission features and are already in use on testbeds.[18–21]

The APLC offers several advantages for terrestrial exoplanet imaging, although it represents a trade-off with other sorts of coronagraph design. APLCs with 2-D binary masks optimized using linear programming can achieve high throughputs with relatively large focal plane masks (FPMs), and therefore relatively large inner working angles (IWAs). For example, Zimmerman *et al.* 2016[22] 2016 find 18% half-max throughput (where half-max throughput is the relative flux of an off-axis source in an aperture encircling half the maximum of the source's point spread function) for a 4 λ/D FPM radius and a dark hole with a 15% bandwidth. Furthermore, the APLC is robust to telescope tip/tilt and stellar angular size in the presence of an obstructed pupil– for example, N'Diaye *et al.* 2016[6] presents APLC designs with 10^9 dark holes that suffer minimal contrast degradation for stars with diameters and tip/tilt errors greater than 0.1 λ/D. In comparison, apodized vortex coronagraphs are able to achieve high throughputs with IWAs of $2-3$ λ/D, but at the expense of tip/tilt and stellar angular size sensitivity in the presence of central obstructions.[23,24]

APLC performance may be improved by changing how the pupil is apodized. Recent results show that some of the task of apodizing an obstructed pupil can be offloaded from the apodizing filter onto pairs of deformable mirrors (DMs) using Active Compensation of Aperture Discontinuities- Optimized Stroke Minimization (ACAD-OSM).[25,26] In particular, as long as a pupil apodizer is present to correct for the central obstruction, DM shapes obtained using ACAD-OSM can compensate for spiders and gaps while only imposing a few % loss to throughput due to distortion of the off-axis planet's point spread function (PSF). Using ACAD-OSM with realistic DM configurations in combination with 1-D apodizing masks (i.e. circularly symmetric masks that only vary in the radial direction) has been shown to produce 2-D dark holes with complex pupils for APLCs, while retaining the sensitivity of the 1-D design to tip/tilt or stellar size.[26]

In this paper, we combine 1-D binary masks with ACAD-OSM to explore the parameter space of APLC designs, with the intention of improving the throughput, bandwidth, or IWA of APLCs designed to deliver 10^{10} contrast with obstructed telescope pupils. By sampling many different configurations of FPM and Lyot stop using a Markov chain Monte Carlo (MCMC) technique, we find 1-D APLCs with throughputs comparable to those obtained with a 2-D binary apodizer, but with IWAs of ~ 3 λ/D. We also report APLC configurations that produce a dark hole with an IWA of ~ 2 λ/D, albeit with lower throughput. These 1-D APLCs are then combined with ACAD-OSM to create dark holes for a complex obstructed pupil, allowing us to demonstrate gains in bandwidth and IWA over previous 2-D binary APLC designs. Since the 1-D binary mask designs we sample with MCMC can be easily combined with DMs to make dark holes with 2-D pupil, we are also able to lay the groundwork for extending our approach to exploring the parameter space of possible 1-D APLC designs to directly optimize the terrestrial exoplanet yield. By optimizing these 1-D designs for yield and then converting them to 2-D apodizations with ACAD-OSM, we will be better able to design versions of the APLC which will maximize our chances of detecting biomarkers with future direct imaging missions.

2. METHODS

We examine the space of APLC designs with pupil pupil-plane apodizations obtained with a combination of binary masks and DM beam shaping. We use a hybrid linear and nonlinear strategy for finding new configurations of APLC that use a circularly symmetric 1-D binary mask to construct a dark hole in the presence of a central obstruction. We probe the space of focal plane mask radius (R_{FPM}), inner Lyot stop radius (R_{ILS}) and outer Lyot stop radius (R_{OLS}) using a modified MCMC algorithm, where for each sampled combination of (R_{FPM}, R_{ILS}, R_{OLS}) we find the linearly optimized binary mask that maximizes transmission. Using this approach, we find regions of ($R_{FPM} \times R_{ILS} \times R_{OLS}$) parameter space with high total energy (T.E.) throughput* From the results of this sampling we select combinations of parameters and masks to use in conjunction with ACAD-OSM with a 2-D pupil. We examine using ACAD-OSM both to compensate for spiders and gaps in the dark hole

*Throughout the paper, we use two definitions of throughput: encircled energy (E.E.) throughput and total energy (T.E.) throughput. E.E. throughput is defined to be the energy from an off-axis companion that is in an aperture of radius 0.7λ/D around the position of the companion in the image plane relative to the energy in the pupil. T.E. throughput is defined to be the total energy in the Lyot plane relative to the energy in the pupil. We use the term 'T.E. throughput' instead of 'transmission' to avoid confusion with the linear quantity being maximized when optimizing the pupil apodizer.

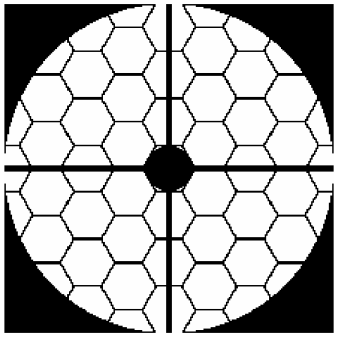

Figure 1. Reference pupil for APLC designs studied in this work. The pupil features a hexagonal segmentation pattern with segment gap widths comparable to the segments in the proposed LUVOIR-B aperture, a central obstruction that is 14% of the pupil radius, and four support struts.

created by the binary mask APLC and to reduce the inner angle of the dark hole (i.e. the smallest angular separation between the on-axis star and off-axis companion such that the contrast is 10^{10} between the inner angle and the outer edge of the dark hole).

2.1 APLC Pupil Apodization Optimization

In order to find a binary mask for an APLC that produces a dark hole with 10^{10} contrast in the image plane, we construct a linear problem that maximizes transmission in the Lyot plane. The detailed derivation for propagation of a coherent source through an APLC and the linear problem that maximizes transmission is given in N'Diaye *et al.* 2015.[6] While we restrict our attention to binary apodizers, the general linear problem in for maximizing apodizer transmission given a target dark hole remains the same as the smooth apodizer case in N'Diaye *et al.* 2015.[6]

Ideally, we would like to optimize the apodizer to maximize the off-axis companion's E.E. throughput. However, this is a computationally expensive non-linear problem. Furthermore, maximizing Lyot plane transmission approximately maximizes E.E. throughput, as long as the coronagraph-induced PSF distortions are minimal. For binary apodizers, we find that as long as the T.E. throughput of the APLC is greater than 50%, PSF distortions impact E.E. throughput by no more than a factor of ~ 2 (see Section 3.2 below).

We use the Gurobi python API to solve the linear problem for optimizing the APLC pupil mask. We use the python wrapper described in N'Diaye et al. 2018,[27] which provides functionality for using the numerical methods found in Gurobi for solving linear programs in python for coronagraphic apodizers.

2.2 ACAD-OSM

Mazoyer *et al.* 2018a[25] showed that pupil beam shaping using ACAD-OSM with a pair of DMs can correct gaps and spiders with only a few % E.E. throughput loss. We use ACAD-OSM in combination with 1-D binary masks to produce dark holes with 10^{10} contrast in the image plane for the pupil shown in Figure 1, which has a 14% central obstruction and a segmentation pattern based on the LUVOIR-B architecture.[28] The pupil we study has elements that impose more stringent design requirements than either the LUVOIR-A or LUVOIR-B pupils currently proposed, allowing us to present results that will be applicable to a large range of obstructed pupil configurations.

ACAD-OSM uses stroke minimization to flatten the wavefront in the telescope pupil with a pair of DMs while minimizing the amplitude (or stroke) of the DM actuators.[25,26,29,30] For our setup, we use hypothetical

DMs with 48x48 actuators with 0.3mm pitch (for a total side length of 14.4mm) spaced 0.3m apart. This setup provides a Fresnel number of 1.3×10^3, which is above the threshold of 5×10^2 found in Mazoyer *et al.* 2018b[26] for minimizing the impact of vignetting on contrast.

Our decision to use a circularly symmetric 1-D binary apodizer to account for the central obstruction and ACAD-OSM for spider and gaps is based on previous success using this strategy to compensate for pupil obstructions. Using DMs to compensate for spiders, gaps, and other small-scale pupil features can be more 'efficient' than pupil apodization, in the sense that the E.E. throughput of a coronagraph combining a 1-D apodizer with DMs is higher than the E.E. throughput of a comparable coronagraph with a 2-D apodizer alone.[25] On the other hand, we found that using ACAD-OSM to correct 'thick' features in the pupil, such as the central obstruction, hexagonal primary mirror boundaries, or using the DMs to replace large sectors of the pupil apodizer with 0 transmission, typically results in worse E.E. throughput performance.[31] We suspect that ACAD-OSM provides nearly optimal throughput performance when compensating for small-scale pupil structures, since the correspondingly small strokes placed on the DMs will tend to produce the flattest possible wavefront, and therefore the least possible distortion of the off-axis companion PSF. However, since we do not optimize for E.E. throughput, it is possible that variant DM beam-shaping approaches may be developed that will provide better throughput performance with larger pupil structures. Therefore, we do not claim that the combined apodizer and DM strategy we adopt in this paper is the final word on the contrast and throughput performance that may be achieved by combining these two approaches to pupil shaping.

We also examine two cases where the inner angle of the dark hole is either the same as or slightly greater than R_{FPM}. In these cases, we attempt to reduce the inner angle of the dark hole using ACAD-OSM. We set up the stroke minimization algorithm in the same way we would otherwise, but instead of defining the dark hole to have the same inner and outer angles as the dark hole produced by the 1-D apodizer in the absence of spiders and gaps, we define the dark hole to have a smaller inner angle. In each case, we defined the target inner angle to be 0.25 λ/D less than R_{FPM}.

2.3 Monte Carlo Parameter Sampling

We use the affine invariant MCMC ensemble sampler implemented in `emcee`[32†] to create MCMC chains that sample the $(R_{FPM} \times R_{ILS} \times R_{OLS})$ parameter space for 1-D APLCs designed to create dark hole with 10^{10} contrast in the presence of a 14% central obstruction. We use 6 walkers in runs consisting of 10^4 samples per walker for 4 target dark holes– each a combination of 10% or 20% bandwidth ($\Delta\lambda$) and inner and outer angles of $2.5 - 10$ λ/D or $4 - 12$ λ/D. We adopt ln (T.E. Throughput) as the MCMC figure-of-merit. For the $2.5 - 10$ λ/D dark hole, we restrict the range of possible R_{FPM}s to $2 - 3.25$ λ/D and for the $4 - 12$ λ/D dark hole we restrict the FPM range to $3 - 6$ λ/D by setting ln (T.E. Throughput) $= -\infty$ for values of R_{FPM} outside these ranges. We also restrict the ranges of R_{ILS} and R_{OLS} to ensure that $R_S \leq R_{ILS} \leq R_{OLS} \leq R_{Pup}$, where R_S is the radius of the central obstruction imposed by the secondary mirror and R_{Pup} is the pupil radius.

3. RESULTS

3.1 APLC Parameter Space Search

We present two-dimensional cuts of our sampling of the $(R_{FPM} \times R_{ILS} \times R_{OLS})$ parameter space for a $4 - 12$ λ/D dark hole in Figure 2. We plot the 20% bandwidth ($\Delta\lambda = 0.2$) case on the top row, and the 10% bandwidth ($\Delta\lambda = 0.1$) case on the bottom. For both cases, we find large portions of parameter space with high T.E. throughput ($\gtrsim 0.5$) apodizers. These high T.E. throughput solutions favor small Lyot stops (i.e. with $R_{ILS} \sim R_S$ and $R_{OLS} \sim R_{Pup}$), suggesting that the FPM is suppressing on-axis starlight efficiently in the Lyot plane, and as a result little of the on-axis starlight needs to be blocked in the Lyot plane. Furthermore, the results in Figure 2 suggest that above a certain threshold, the size of the FPM does not limit T.E. throughput performance. For a 20% bandwidth, this threshold appears to be about 3.25 λ/D, while relaxing the bandwidth requirement to 10% reduces this threshold to ~ 3 λ/D.

Analogous two-dimensional cuts for APLC configurations designed to create a $2.5 - 10$ λ/D dark hole with bandwidths of either 10% or 20% are shown in Figure 3. We find that high T.E. throughput solutions exist for the

[†]http://dfm.io/emcee/current/

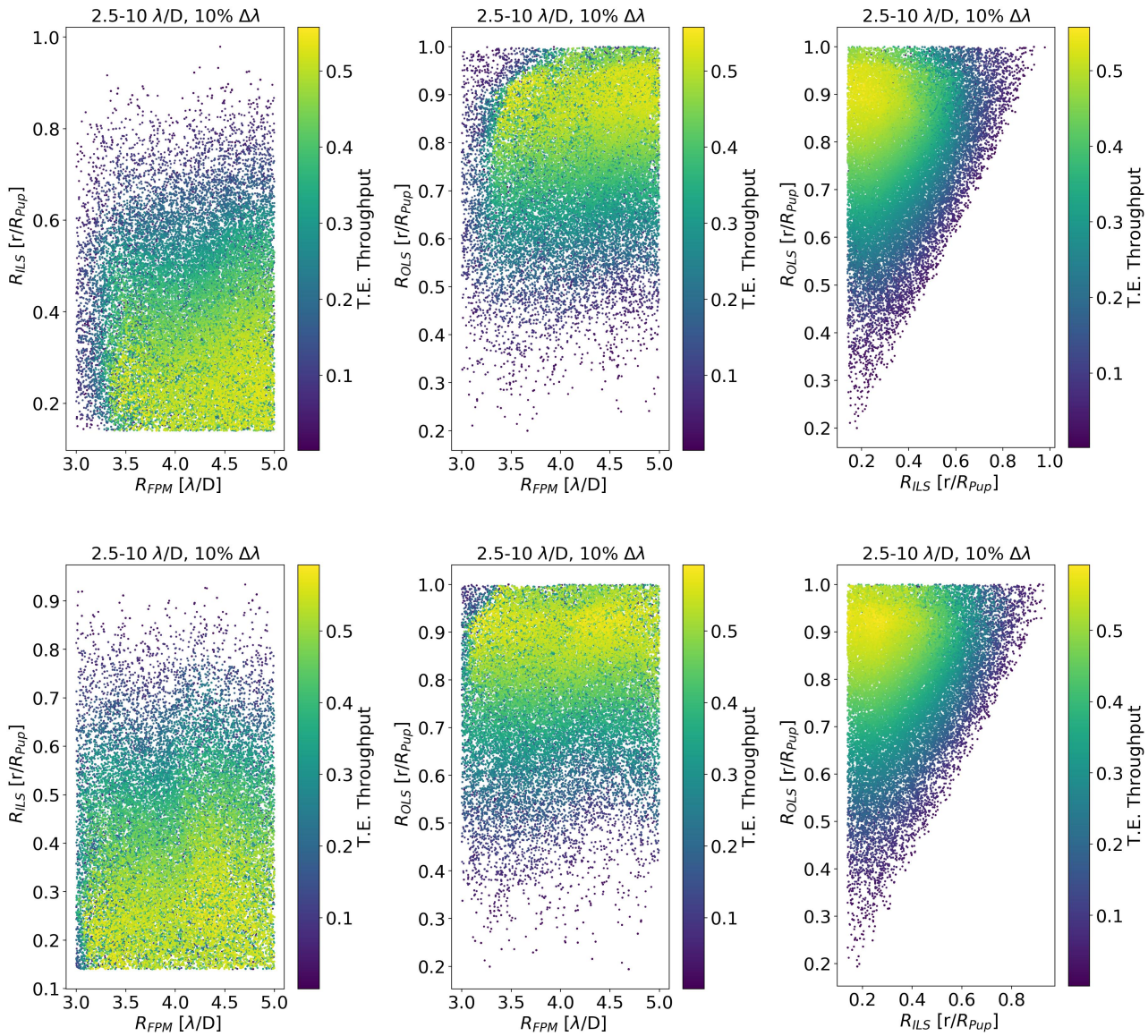

Figure 2. *Top Row:* Scatter plots showing the MCMC sampling of 2-D cuts of ($R_{FPM} \times R_{ILS} \times R_{OLS}$) parameter space for APLCs designed to create a 10^{10} dark hole at $4-12$ λ/D with a bandwidth of 20%. The plot on the left shows the distribution of sampled combinations of R_{FPM} and R_{ILS}, the plot in center R_{FPM} and R_{OLS}, and the plot at right R_{ILS} and R_{OLS}. The color of each point corresponds to the T.E. throughput of the optimal coronagraph for the sampled parameters. *Bottom Row:* Analogous plots for a $4-12$ λ/D dark hole with a bandwidth of 10%.

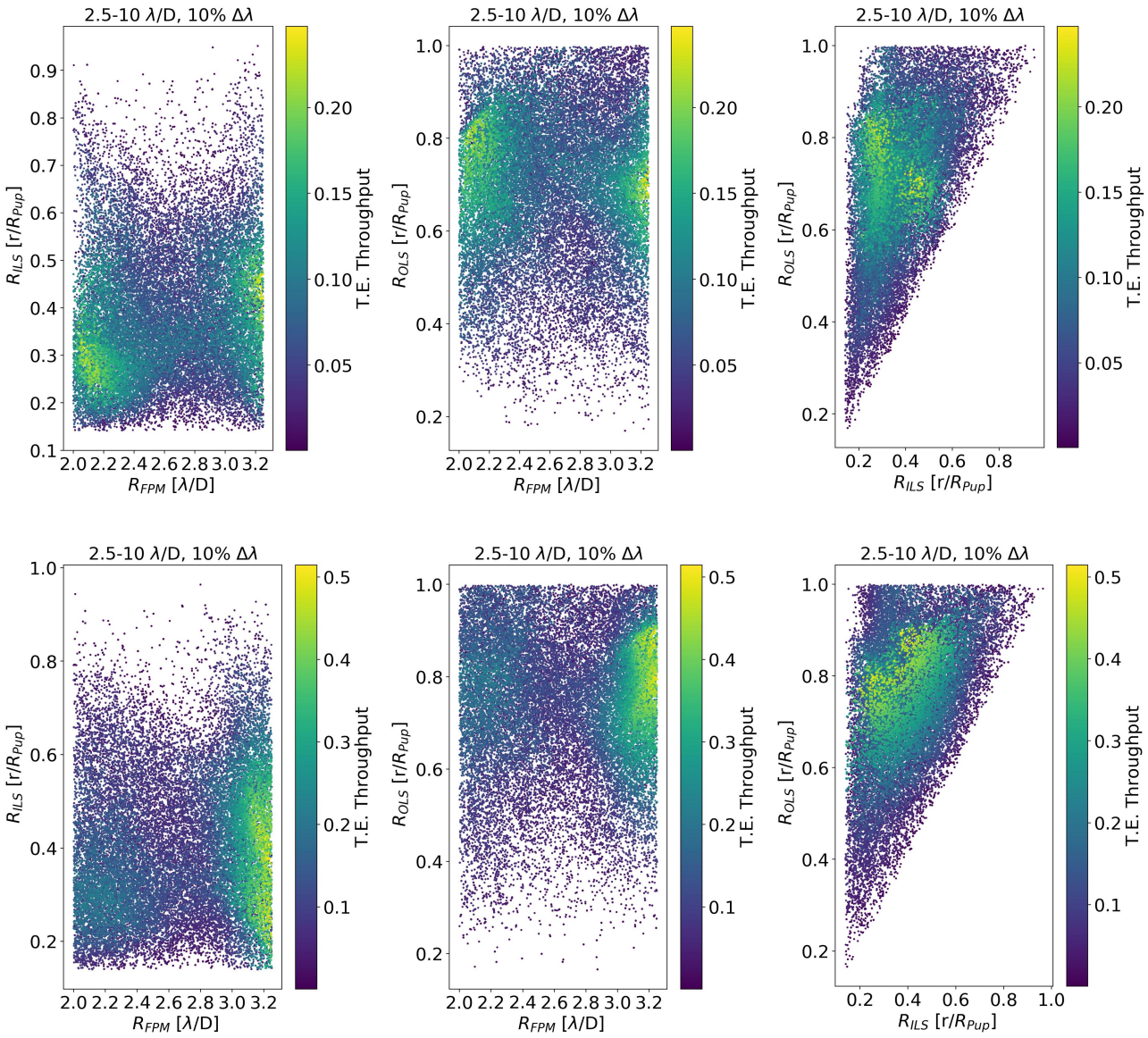

Figure 3. *Top Row:* The same set of plots as in Figure 2, this time for a $2.5-10$ λ/D dark hole with a bandwidth of 20%. *Bottom Row:* Analogous plots for a $2.5-10$ λ/D dark hole with a bandwidth of 10%.

10% bandwidth case; however, the Lyot stops (both inner and outer) for these APLCs are significantly larger– we find that all sampled APLC configurations with T.E. throughputs in excess of 50% have $R_{ILS} \gtrsim 0.37 R_{Pup}$ and $R_{OLS} \lesssim 0.9 R_{Pup}$. Our results demonstrate that the optimal combination of Lyot stop sizes is a function of the desired dark hole produced by the coronagraph, with more stringent dark hole requirements requiring more of the Lyot plane to be blocked.

Unlike coronagraphs optimized for a $4-12$ λ/D dark hole, we find that in the $2.5-10$ λ/D case T.E. throughput is a complicated function of FPM radius. T.E. throughput peaks in two regions, centered around $R_{FPM} \sim 2.1$ λ/D and $R_{FPM} \gtrsim 3$ λ/D. T.E. throughput for the $R_{FPM} \gtrsim 3$ λ/D is $\sim 50\%$ when $\Delta\lambda = 0.1$, but

falls to $\sim 25\%$ when $\Delta\lambda = 0.2$. On the other hand, T.E. throughput for the $R_{FPM} \sim 2.1$ λ/D designs is $\sim 25\%$ for both bandwidths. While the family of 'small IWA' APLC designs with $R_{FPM} \sim 2$ λ/D have modest T.E. throughput (and correspondingly diminished E.E. throughput) relative to binary-mask APLCs in the literature that have been optimized for complex, centrally obstructed apertures, their large bandwidths and small IWAs make them an interesting new set of potential APLC configurations.

Since the T.E. throughput maxima are located near to the edges of the search volume for R_{FPM}, we performed a subsequent test where we examined APLCs that have $R_{FPM} \leq 2.7$ λ/D and a $2.5 - 10$ λ/D dark hole. We did not perform a similar test exploring the range $R_{FPM} > 3.25$, since for these cases we would not actually be improving the IWA of the APLC. We do not find that we missed any higher T.E. throughput cases at smaller R_{FPM}. Since probing to lower R_{FPM}s does not reveal higher throughput solutions in the 10% bandwidth case, we do not go on to explore the 20% bandwidth case.

Our MCMC exploration of APLC parameters reveals that the IWA of a centrally obstructed APLC can be reduced to ~ 3 λ/D without a significant loss of throughput. It also reveals a new set of 'small IWA' APLCs that are potentially useful for expanding the search volume for terrestrial exoplanets. As we discuss when presenting DM optimizations (section 3.2) and again in the discussion, the lower throughputs for the small IWA designs we find are offset by their ability to accommodate larger (e.g. 20%) bandwidths and to access IWAs as small as 2 λ/D.

3.2 DM Optimization

We used the APLC parameter space search to identify several interesting cases that, when combined with ACAD-OSM DM beam shaping to produce a 2-D apodization for a complex pupil, represent possible avenues for improving APLC performance. First, we examined a coronagraph producing a 4-12 λ/D dark hole with a 20% bandwidth, and a coronagraph producing a 2.5-10 λ/D dark hole with a 10% bandwidth. These two designs have high T.E. throughput ($\gtrsim 50\%$), and alternately improve the bandwidth or the IWA of binary-mask only designs. Seeking to extend both the APLC IWA and bandwidth at the expense of throughput, we also examined a solution with a 2.5-10 λ/D dark hole and 20% bandwidth. Finally, we considered two other cases where we could potentially use DMs to reduce the inner angle of the dark hole to below the FPM radius.

We show the 1-D apodization and broadband dark hole for our first case, an APLC with a 4-12 λ/D dark hole and 20% bandwidth, in Figure 4. The inner and outer Lyot stops have radii of $0.24R_{Pup}$ and $0.93R_{Pup}$, respectively, and are shown on the left-hand plot as black vertical dashed lines (the red vertical dashed line shows the radius of the central obstruction, $0.14R_{Pup}$). The FPM radius is 4.5 λ/D, and is shown on the right-hand plot as a vertical dashed line as well. We chose to examine an APLC configuration where R_{FPM} is greater than the inner angle of the dark hole, since in N'Diaye *et al.* 2015[6] having the inner angle be less than R_{FPM} was shown to tend to preserve tip/tilt robustness in the cases they studied.

In Figure 5 we show the DM shapes used create the 2-D dark hole in the presence of gaps and spiders, along with the off-axis E.E. throughput curves for the coronagraph both before and after the DM shapes are applied. These curves show the amount of useable throughput the combined coronagraph and telescope provides for a planet or other off-axis source as a function of its angular separation from an on-axis star. As is typical for an APLC, the off-axis throughput curve is very nearly a step-function, so we can define a single value for the E.E. throughput, which in this case is 18%. As with all the E.E. throughput values we discuss in this paper, we have defined throughput relative to the total energy of the source in the pupil. Without the coronagraph, the E.E. throughput of a point source given our pupil would be 57.2%, and if the pupil were apodized with a uniform greyscale filter with a T.E. throughput of 58%, the E.E. throughput would be 33%. Therefore, the shape of the apodizer and Lyot stop distorts the off-axis PSF, and causes the E.E. throughput to drop by $\sim 15\%$. The DMs further slightly distort the PSF and reduce the throughput by $\sim 2\%$.

We present analogous plots to Figures 4 and 5 in Figures 6 and 7 for the 2.5-10 λ/D dark hole with 10% bandwidth case, and in figures 8 and 9 for the 20% bandwidth case. For the 10% case, $R_{ILS} = 0.37R_{Pup}$, $R_{OLS} = 0.89R_{Pup}$ and $R_{FPM} = 3.24$ λ/D. For the 20% case, $R_{ILS} = 0.35R_{Pup}$, $R_{OLS} = 0.81R_{Pup}$, and $R_{FPM} = 2.07$ λ/D. In each case, we chose examples from among the APLC designs found by our MCMC runs where the inner angle of the dark hole is inside the FPM radius– in the first case, the 2.5 λ/D required by the

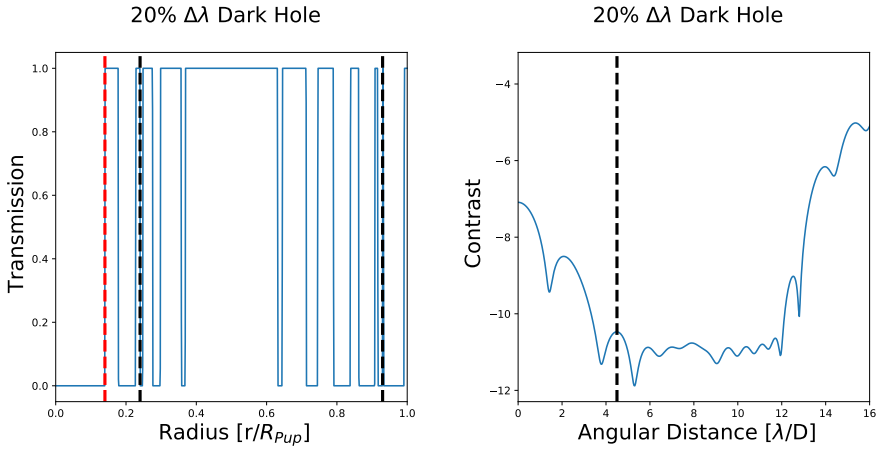

Figure 4. *Left:* Radial profile of the circularly symmetric binary pupil mask for the case of an APLC creating a $4-12$ λ/D dark hole with a bandwidth of 20% and a FPM radius of 4.5 λ/D. The blue solid line shows the transmission as a function of the radius in the pupil plane, in units relative to R_{Pup}. The dashed red line depicts the radius of the central obstruction, and the dashed black lines depict the inner and outer Lyot stop radii. *Right:* Radial profile of the dark hole generated by the coronagraph. The solid blue line shows contrast as a function of angular separation from the on-axis star, and the black dashed line denotes R_{FPM}.

constraints of the linear program is inside the 3.24 λ/D FPM radius, while in the second case, the effective inner angle for the APLC configuration turns out to be 1.8 λ/D. For the 20% bandwidth coronagraph, we opted to study a design with $R_{FPM} \sim 2$ λ/D since the T.E. throughput for $R_{FPM} \sim 2$ λ/D and $R_{FPM} \sim 3.25$ λ/D are comparable, but the $R_{FPM} \sim 2$ λ/D has a significantly smaller IWA.

The E.E. throughput of the 10% case is similar to the 4-12 λ/D, 20% bandwidth APLC, albeit with a smaller IWA. The E.E. throughput of this coronagraph is 16% after the DM solution is applied. The 2.5-10 λ/D, 20% bandwidth case; however, has an apodizer and Lyot stop that provide less than half the T.E. throughput of the other two cases, and creates a significantly greater PSF distortion. A uniform greyscale apodizer with 23% T.E. throughput would provide 13% E.E. throughput, but the APLC we present has an E.E. throughput of 2.9% after accounting for the DMs. In each case, the DMs only degrade the throughput a few percent– 2% in the 10% bandwidth case and 0.4% in the 20% bandwidth case.

3.2.1 Decreasing the Dark Hole Inner Angle

We explored two cases where the inner angle of the dark hole was slightly larger than the FPM radius, and tried to use the DMs to push the inner angle of the dark hole to be 0.25 λ/D smaller than R_{FPM}. We first examined an apodizer optimized to dig a dark hole between 4-12 λ/D in a 10% bandwidth with $R_{FPM} = 3.18$ λ/D. For the central obstruction alone, this apodizer creates a dark hole with an effective inner angle of 3.5 λ/D while using a Lyot stop with $R_{ILS} = 0.26R_{Pup}$ and $R_{OLS} = 0.94R_{Pup}$. The small Lyot stop for this APLC is a useful design feature, since it has a nearly negligible impact on the spatial resolution of the combined telescope and coronagraph. We attempted using ACAD-OSM to make a 2-D dark hole with an inner angle of 2.9 λ/D. Using this approach, we obtain about a factor of 1.2 increase in E.E. throughput (20% vs 16%) over our previous ~ 3 λ/D coronagraph, although some residual flux above 10^{-10} remains in the dark hole. We defer the question of whether this design retains tip/tilt stability to a later paper, and report on this result here as a promising avenue for using DMs to recover throughput in APLC coronagraphs apodized with both binary masks and DMs.

A similar exercise using an APLC with $R_{FPM} = 2.1$ λ/D, $R_{ILS} = 0.25R_{Pup}$ and $R_{OLS} = 0.82R_{Pup}$ resulted in a throughput gain of about a factor of 1.2 over the previous ~ 2 λ/D coronagraph with 20% bandwidth as well (3.5% vs 2.9%). However, in this case, it appears using ACAD-OSM to calculate DM shapes did not reduce the dark hole inner angle from it's original 2.05 λ/D to 1.85 λ/D.

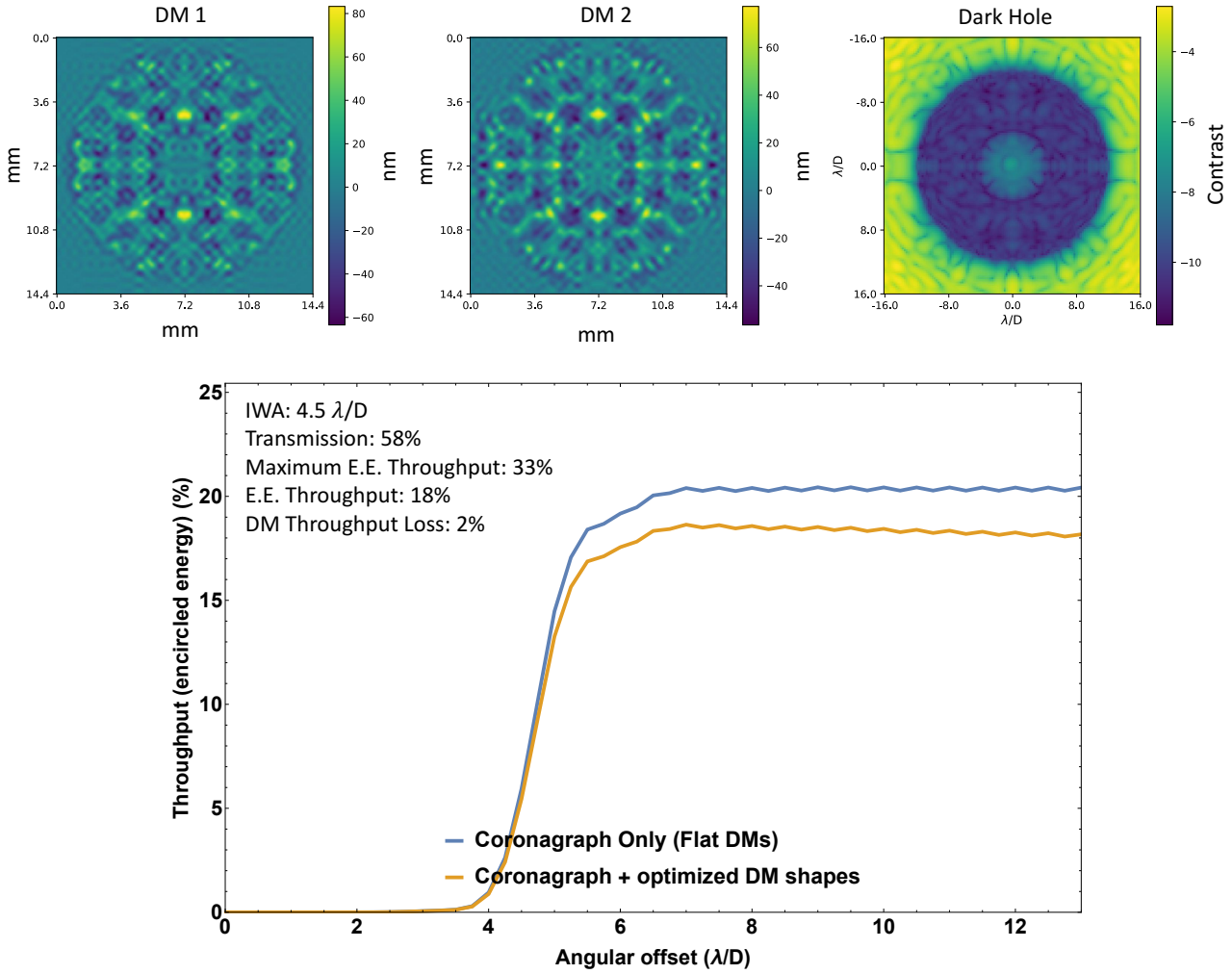

Figure 5. *Top Row:* DM calculated by ACAD-OSM for the APLC in Figure 4 and the pupil in 1 are shown in the left two plots, and the 2-D dark hole for the full coronagraph is shown in the rightmost plot. DM heights are given in units of nm. *Bottom Row:* E.E. throughput as function of angular separation (in units of λ/D) from the on-axis star. The blue curve depicts throughput before the ACAD-OSM solution is applied to the DMs, and the orange curve depicts throughput after.

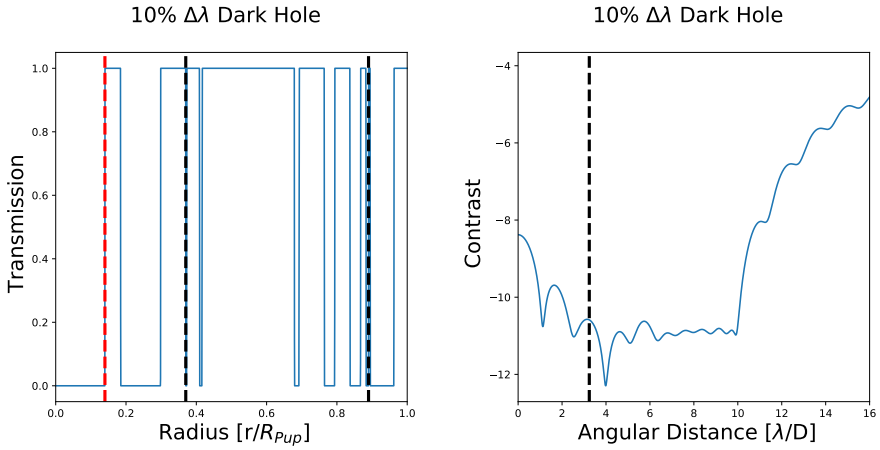

Figure 6. *Left:* Radial profile of the circularly symmetric binary pupil mask for the case of an APLC creating a $2.5-10$ λ/D dark hole with a bandwidth of 10% and a FPM radius of 3.24 λ/D. The blue solid line shows the transmission as a function of the radius in the pupil plane, in units relative to R_{Pup}. The dashed red line depicts the radius of the central obstruction, and the dashed black lines depict the inner and outer Lyot stop radii. *Right:* Radial profile of the dark hole generated by the coronagraph. The solid blue line shows contrast as a function of angular separation from the on-axis star, and the black dashed line denotes R_{FPM}.

4. DISCUSSION

By using circularly symmetric 1-D binary pupil masks to compensate for central obstructions in concert with DM beam shaping to account for gaps and spiders, we find that we improve both the IWA and bandwidth of APLCs designed for exo-Earth imaging on future space telescopes. These improvements come in part from being able to expand our search of APLC parameter space using a combination of MCMC to sample FPM and Lyot stop sizes and linear programming to calculate transmission-maximizing binary masks and in part from being able to offload the work of correcting the 2-D dark hole onto DMs with a minimal loss of E.E. throughput. Our analysis points to several possible avenues that may allow for further improvements to the APLC using the strategy of combining apodizers and DMs employed in this paper. We can also expand our parameter space search to encompass quantities such as dark hole bandwidth and inner angle, and begin to look at optimizing coronagraphs for terrestrial exoplanet yield.

One factor limiting our ability to find high-performance 1-D apodizers is our reliance on linear programming to find binary masks that maximize transmission for a given combination of FPM and Lyot stop. The high transmission apodizers we studied in this paper (see Figures 4 and 6) produce E.E. throughputs that are about half of what would be produced by a flat grey apodizer with the same transmission, but when we look at the small IWA family of APLCs with $\sim$ 25% T.E. throughput, we only recover about a quarter of the possible E.E. throughput. While it may be safe to assume maximizing transmission will maximize throughput for high-transmission binary masks, this assumption quickly breaks down as the masks become less transmissive.

One possible route to improving E.E. throughput in APLCs would be to modify how the binary mask is optimized. While directly optimizing the pupil for E.E. throughput would be prohibitively computationally expensive for all but the coarsest pupil samplings, it may be possible to develop a proxy linear problem by appropriately weighting the pupil and maximizing transmission.

A second possibility would be to replace the binary apodizer with a smooth apodizer. Binary apodizers with large sectors with a transmission of either 0 or 1 represent a significant deviation from a uniform pupil, and may distort the PSF. Smooth masks may allow for apodizer solutions that are closer to a uniformly flat pupil, and therefore may have higher E.E. throughput. Micro-dot masks that approximate masks with smoothly varying transmission have been used on ground-based coronagraphs and are being investigated for the vector vortex coronagraph, and may be useful for improving APLC E.E. throughput performance as well.[9,33–35]

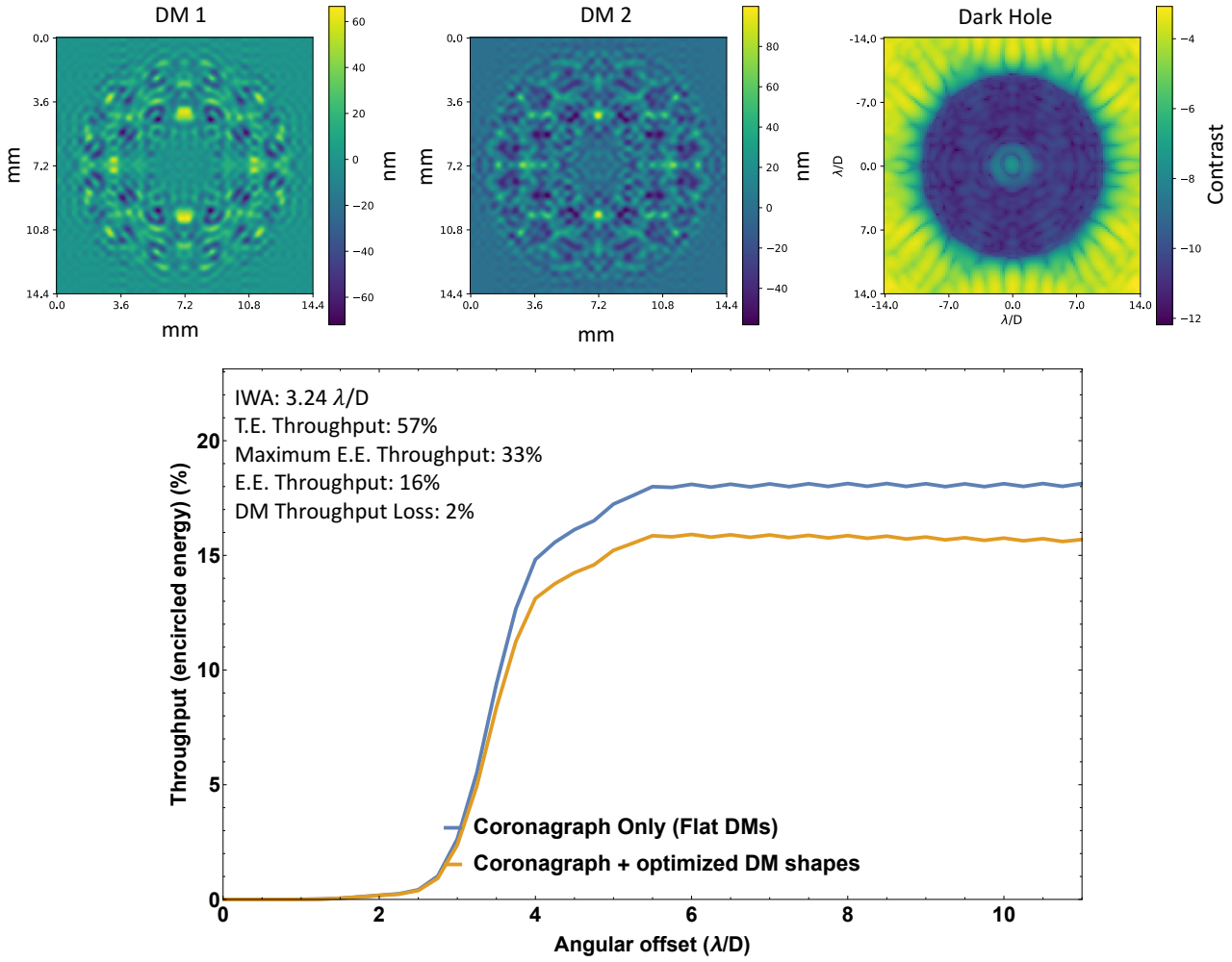

Figure 7. *Top Row:* DM calculated by ACAD-OSM for the APLC in Figure 6 and the pupil in 1 are shown in the left two plots, and the 2-D dark hole for the full coronagraph is shown in the rightmost plot. DM heights are given in units of nm. *Bottom Row:* E.E. throughput as function of angular separation (in units of λ/D) from the on-axis star. The blue curve depicts throughput before the ACAD-OSM solution is applied to the DMs, and the orange curve depicts throughput after.

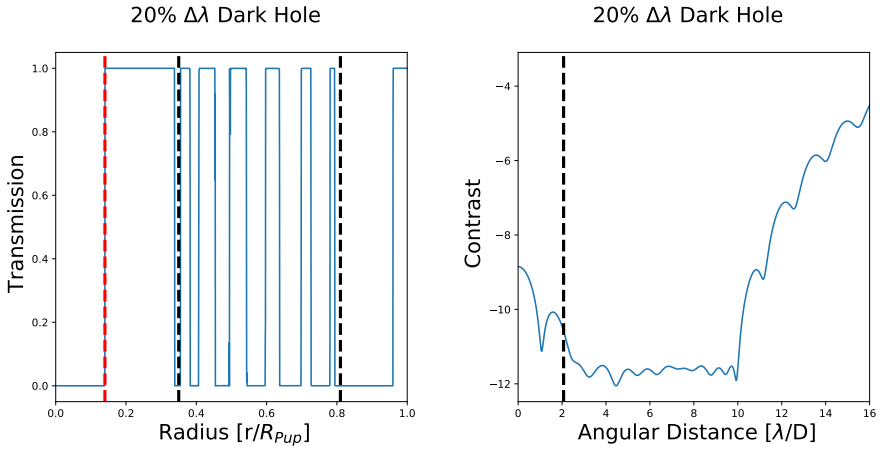

Figure 8. *Left:* Radial profile of the circularly symmetric binary pupil mask for the case of an APLC creating a $2.5-12$ λ/D dark hole with a bandwidth of 20% and a FPM radius of 2.07 λ/D. The blue solid line shows the transmission as a function of the radius in the pupil plane, in units relative to R_{Pup}. The dashed red line depicts the radius of the central obstruction, and the dashed black lines depict the inner and outer Lyot stop radii. *Right:* Radial profile of the dark hole generated by the coronagraph. The solid blue line shows contrast as a function of angular separation from the on-axis star, and the black dashed line denotes R_{FPM}.

Our results also suggest that it may be possible to offload improving the contrast on parts of the dark hole to the DMs using ACAD-OSM. We have shown that small improvements in contrast may be possible by slightly relaxing the requirements for the inner angle of the dark hole, and using the DMs to extend the dark hole inside the FPM. In an upcoming publication we plan to fully explore the strategy of using the DMs to extend the dark hole, and to address the impact this strategy has on tip/tilt stability.

4.1 Yield Optimization

The MCMC framework we used to explore the space of $(R_{FPM} \times R_{ILS} \times R_{OLS})$ can be expanded to many other parameters, which in turn can allow us to optimize 1-D coronagraphs for terrestrial exoplanet yield. Unlike maximizing either T.E. throughput or E.E. throughput, the yield of a coronagraphic mission is the actual astrophysical quantity of interest that will determine either the mission's success finding biosignatures or its ability to place upper limits on the incidence of biosignature detection. We approximate terrestrial exoplanet yields for APLCs using a toy model based on the parametric analysis conducted in Stark *et al.* 2014.[36] The exponential factors for each term in the analysis are typical values from Stark *et al.* 2014,[36] and we use them here as a proof of concept for optimizing yield. We model the yield Y as

$$Y = N\frac{T^{0.35}\Delta\lambda^{0.35}R_{OLS}^{0.7}}{IWA}, \tag{1}$$

where N is a normalization factor, and T is throughput (which we assume to be the E.E. throughput). In the original parametric analysis, T as a function of star-planet angular separation was modeled as a step function that jumps from 0 to T at the IWA, which is similar to the E.E. throughput of the APLC designs studied here. When yield is being calculated for missions such as LUVOIR, the values will need to be carefully modeled based on observatory parameters such as the telescope pupil and on prior information about the systems being studied such as the expected amount of exozodiacal light. The $R_{OLS}^{0.7}$ term arises from the dependence of the planet signal-to-noise on the size of the photometric aperture used to extract signal, which will increase for larger outer Lyot stops. Based on the values in Stark *et al.* 2014[36] for a 12m class mission, if we use a 10^{10} contrast coronagraph with $T = 0.2$ and $\Delta\lambda = 0.2$ and IWA $= 2$ λ/D, and that the typical system has ~ 3 exozodis, the yield will be ~ 34, we estimated that $N = 179$. We scaled this up for an inscribed pupil diameter of 13.5m, so $N = 226.5$.

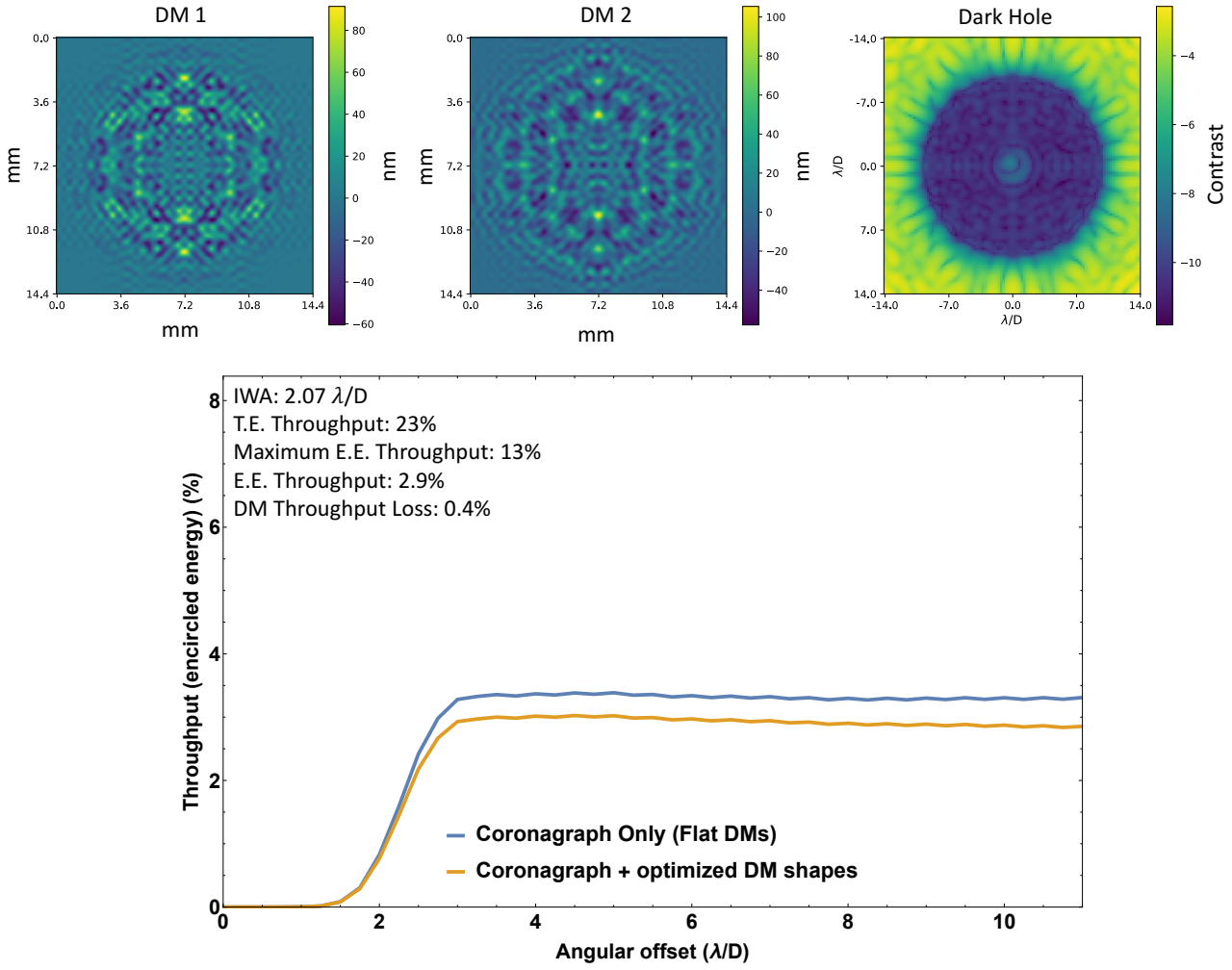

Figure 9. *Top Row:* DM calculated by ACAD-OSM for the APLC in Figure 8 and the pupil in 1 are shown in the left two plots, and the 2-D dark hole for the full coronagraph is shown in the rightmost plot. DM heights are given in units of nm. *Bottom Row:* E.E. throughput as function of angular separation (in units of λ/D) from the on-axis star. The blue curve depicts throughput before the ACAD-OSM solution is applied to the DMs, and the orange curve depicts throughput after.

Using the expression in Equation 1, we find that all of the APLC designs studied in Section 3.2 have a relatively similar yield; however, reducing the IWA improves yield by as much as 30% (given our model for Y), even when it is at the expense of bandwidth or throughput. We summarize the individual yields in Table 1, all of which are between 14 and 18. However, since these coronagraphs have IWAs between ~ 2 λ/D and 4.5 λ/D, these yields are being driven by planet detections at different distances. It is also interesting to note the comparable performance of the 'small IWA' family of APLCs with the other designs we studied, despite these coronagraphs having a factor of $\sim 4-6$ lower E.E. throughput.

We used MCMC to sample 1-D APLC designs with 14% central obstructions in ($R_{FPM} \times R_{OLS} \times R_{ILS} \times \Delta\lambda \times R_{IA}$) space, where R_{IA} is the dark hole inner angle, and look for coronagraphs which maximize Y. As noted above, since the off-axis throughput curve of an APLC is nearly a step function on either side of R_{FPM}, it is relatively straightforward to approximate T in Equation 1, as opposed to the vortex coronagraph, for example, where off-axis throughput varies smoothly as a function of star-companion angular separation.[8] We chose to estimate T as a function of T.E. throughput based on the E.E. throughput of the coronagraphs we studied in this paper, using the formula

$$T = \begin{cases} 0.174 T_{T.E.} & \text{if } T_{T.E.} < 0.23 \\ 0.52 T_{T.E.} - 0.08 & \text{if } 0.23 \leq T_{T.E.} < 0.63 \\ 0.87 T_{T.E.} - 0.30 & \text{if } 0.63 \leq T_{T.E.}. \end{cases} \quad (2)$$

Since we allowed $\Delta\lambda$ to reach values as large as 0.5, we also increased the bandpass sampling from 5 to $\mathbf{max}\,(5, \mathbf{round}\,(\Delta\lambda/0.025))$, to ensure that we avoided under-sampling the band for large bandwidths.

After our initial run of 10^4 samples we found there were two regions of high yield. In order to adequately sample each region, we performed two runs of 10^4 samples for both cases, with one run restricted to $R_{FPM} < 3$ λ/D and the other restricted to 3 λ/D $\leq R_{FPM} \leq 8$ λ/D. Figure 10 shows the results of these two runs stitched together into a single plot, where we have plotted the distribution of yields against $\Delta\lambda$ and the effective IWA, defined to be the maximum of either R_{FPM} or R_{IA}. One region of high yield corresponds to the 'small IWA' family of coronagraphs we found earlier. The designs in this region with optimal yield have an effective IWA of ~ 2 λ/D and a bandwidth of $\sim 20\%$. If we can find ways to improve E.E. throughput for an APLC as a function of T.E. throughput, these designs will produce the highest yields of any coronagraph in the parameter space we surveyed.

The other region appears to follow a slope in effective IWA - $\Delta\lambda$ space, and the optimal yield in this region is close to IWA = 4 λ/D and $\Delta\lambda = 0.3$, for both the optimistic and realistic E.E. throughput cases. From a coronagraphic design perspective, these plots show that we can effectively increase the bandwidth to 0.5 or even larger and obtain high-yield instruments. In order to exploit this portion of parameter space, it will be necessary to be able to maintain wavefront stability over bandpasses of this size. However, if this hurdle can be overcome, our results suggest that IWA $\gtrsim 4$ λ/D APLCs with $\gtrsim 30\%$ bandwidths could be useful, for example, for rapid spectral characterization of nearby exoplanets. Furthermore, the 'ridgeline' of high yield followed by this second region passes slightly outside the combination of IWA and bandwidths that were examined when producing 2-D binary mask APLCs, which focused on designs with an IWA ~ 4 λ/D and $\Delta\lambda \sim 10-20\%$.[17]

Modeling yields parametrically for a given combination of primary and secondary mirrors and using MCMC to maximizing model yields has the potential to improve APLC coronagraph performance for planned future

Table 1. Summary of Yields in APLC Designs

R_{FPM} [λ/D]	$\Delta\lambda$	Yield
4.50	0.2	14
3.24	0.1	15
3.18	0.1	18
2.10	0.2	17
2.07	0.2	16

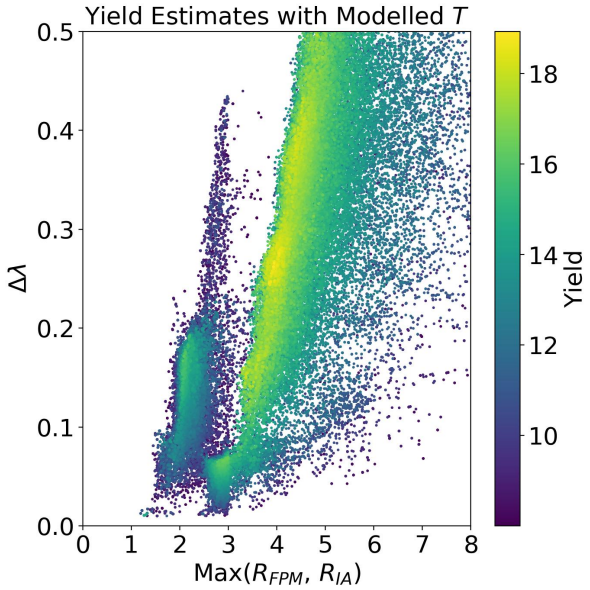

Figure 10. Scatter plot showing the two MCMC runs sampling yield assuming a model for T based on results obtained in Section 3.2 for $T_{E.E.}$. The two runs have been stitched into a single plot, showing the distribution of yields as a function of effective IWA and bandwidth. We plot all samples with a yield ≥ 8. Effective IWA is plotted on the x-axis and is defined in this plot to be the maximum of either R_{FPM} or the dark hole inner angle, R_{IA}.

missions such as LUVOIR. Importantly, APLC designs with yields near the peak of the distribution seen in Figure 10 exist for IWAs spanning the range of ~ 2 to $\gtrsim 4$ λ/D. Coronagraphs with smaller IWAs and more modest throughputs will be able to observe more distant planets, while coronagraphs with higher IWAs and larger throughputs will be able to observe nearby volumes more completely, suggesting that e.g. an APLC with IWA $= 2$ λ/D and $\Delta\lambda = 0.2$ could be combined with a higher throughput APLC with IWA $= 3.2$ λ/D and $\Delta\lambda = 0.1$ on a single mission to produce a higher overall yield. Subsequent efforts will entail careful modeling of the exponents in the expression for Y, the inclusion of additional design parameters, such as contrast, and modeling the yield of multi-coronagraph missions.

5. CONCLUSION

We combined 1-D circularly symmetric binary pupil masks with DM beam shaping using ACAD-OSM to create 2-D apodizations for APLCs designed for complex pupils with central obstructions. We focused our study on a hypothetical pupil with a 14% central obstruction, spiders, and hexagonal primary mirror segments patterned on the proposed LUVOIR-B primary. We constructed our test pupil to be more difficult to apodize than the proposed LUVOIR-A pupil, in order to find results that are applicable not only to LUVOIR-A, but potentially other telescope designs as well.

Using a new approach to find optimal APLC design parameters that combines linear programming to obtain binary masks with an MCMC-based algorithm to sample R_{FPM}, R_{ILS}, and R_{OLS}, we found 1-D apodizers that can provide $\sim 50\%$ T.E. throughput for APLCs with an IWA of ~ 3 λ/D and $\Delta\lambda = 0.1$ and $\sim 25\%$ T.E. throughput for APLCs with an IWA of ~ 2 λ/D and $\Delta\lambda = 0.2$. For the former, the 2-D APLCs we studied have an E.E. throughput of $16 - 20\%$, while the latter have an E.E. throughput of $3 - 4\%$. However, despite the small E.E. throughput of these small IWA coronagraph designs, the fact that they have an IWA ~ 2 λ/D and can have bandwidths of 20% implies that they can potentially still obtain high planet yields.

Our method for designing APLCs both opens up the parameter space of potentially useful APLC designs and lays the groundwork for optimizing an APLC for terrestrial exoplanet yield. We demonstrated using our 1-D design approach to find APLCs that maximize a simple expression approximating planet yield. We found

two families of high-yield solutions, one with small IWAs (corresponding to the $R_{FPM} \sim 2$ λ/D coronagraphs discussed in Section 3.1), and one occupying a ridgeline in IWA-$\Delta\lambda$ that runs from IWA ~ 3 λ/D, $\Delta\lambda \sim 0.05$ to IWA ~ 5 λ/D, $\Delta\lambda \sim 0.5$. Fully exploiting this method will require carefully modeling the yield for specific telescopes and physical assumptions; however, doing so will allow us to improve the yield of individual APLC designs or combinations of APLC coronagraphs put forward for upcoming space telescopes.

ACKNOWLEDGMENTS

This work is supported by the National Aeronautics and Space Administration under Grants NNX12AG05G and NNX14AD33G issued through the Astrophysics Research and Analysis (APRA) program (PI: R. Soummer) and by Jet Propulsion Laboratory subcontract No.1539872 (Segmented-Aperture Coronagraph Design and Analysis; PI: R. Soummer). The authors would also like to acknowledge useful discussions with Anand Sivaramakrishnan and A.J. Riggs.

REFERENCES

[1] Stark, C. C., Roberge, A., Mandell, A., Clampin, M., Domagal-Goldman, S. D., McElwain, M. W., and Stapelfeldt, K. R., "Lower Limits on Aperture Size for an ExoEarth Detecting Coronagraphic Mission," *ApJ* **808**, 149 (Aug. 2015).

[2] Bolcar, M. R., Balasubramanian, K., Clampin, M., Crooke, J., Feinberg, L., Postman, M., Quijada, M., Rauscher, B., Redding, D., Rioux, N., Shaklan, S., Stahl, H. P., Stahle, C., and Thronson, H., "Technology development for the Advanced Technology Large Aperture Space Telescope (ATLAST) as a candidate large UV-Optical-Infrared (LUVOIR) surveyor," in [*Optics for EUV, X-Ray, and Gamma-Ray Astronomy VII*], *proc. SPIE* **9602**, 960209 (Sept. 2015).

[3] Dalcanton, J., Seager, S., Aigrain, S., Battel, S., Brandt, N., Conroy, C., Feinberg, L., Gezari, S., Guyon, O., Harris, W., Hirata, C., Mather, J., Postman, M., Redding, D., Schiminovich, D., Stahl, H. P., and Tumlinson, J., "From Cosmic Birth to Living Earths: The Future of UVOIR Space Astronomy," *ArXiv e-prints* (July 2015).

[4] Wang, J., Mawet, D., Hu, R., Ruane, G., Delorme, J.-R., and Klimovic, N., "Baseline Requirements For Detecting Biosignatures with the HabEx and LUVOIR Mission Concepts," *ArXiv e-prints* (June 2018).

[5] Soummer, R., "Apodized Pupil Lyot Coronagraphs for Arbitrary Telescope Apertures," *ApJL* **618**, L161–L164 (Jan. 2005).

[6] N'Diaye, M., Pueyo, L., and Soummer, R., "Apodized Pupil Lyot Coronagraphs for Arbitrary Apertures. IV. Reduced Inner Working Angle and Increased Robustness to Low-order Aberrations," *ApJ* **799**, 225 (Feb. 2015).

[7] Foo, G., Palacios, D. M., and Swartzlander, Jr., G. A., "Optical vortex coronagraph," *Optics Letters* **30**, 3308–3310 (Dec. 2005).

[8] Mawet, D., Riaud, P., Absil, O., and Surdej, J., "Annular Groove Phase Mask Coronagraph," *ApJ* **633**, 1191–1200 (Nov. 2005).

[9] Ruane, G., Jewell, J., Mawet, D., Pueyo, L., and Shaklan, S., "Apodized vortex coronagraph designs for segmented aperture telescopes," in [*Advances in Optical and Mechanical Technologies for Telescopes and Instrumentation II*], *proc. SPIE* **9912**, 99122L (July 2016).

[10] Fogarty, K., Pueyo, L., Mazoyer, J., and N'Diaye, M., "Polynomial Apodizers for Centrally Obscured Vortex Coronagraphs," *AJ* **154**, 240 (Dec. 2017).

[11] Ruane, G., Mawet, D., Mennesson, B., Jewell, J., and Shaklan, S., "Vortex coronagraphs for the Habitable Exoplanet Imaging Mission concept: theoretical performance and telescope requirements," *Journal of Astronomical Telescopes, Instruments, and Systems* **4**, 015004 (Jan. 2018).

[12] Guyon, O., "Phase-induced amplitude apodization of telescope pupils for extrasolar terrestrial planet imaging," *A&A* **404**, 379–387 (June 2003).

[13] Traub, W. A. and Vanderbei, R. J., "Two-Mirror Apodization for High-Contrast Imaging," *ApJ* **599**, 695–701 (Dec. 2003).

[14] Guyon, O., Pluzhnik, E. A., Galicher, R., Martinache, F., Ridgway, S. T., and Woodruff, R. A., "Exoplanet Imaging with a Phase-induced Amplitude Apodization Coronagraph. I. Principle," *ApJ* **622**, 744–758 (Mar. 2005).

[15] Guyon, O., Hinz, P. M., Cady, E., Belikov, R., and Martinache, F., "High Performance Lyot and PIAA Coronagraphy for Arbitrarily Shaped Telescope Apertures," *ApJ* **780**, 171 (Jan. 2014).

[16] N'Diaye, M., Soummer, R., Pueyo, L., Carlotti, A., Stark, C. C., and Perrin, M. D., "Apodized Pupil Lyot Coronagraphs for Arbitrary Apertures. V. Hybrid Shaped Pupil Designs for Imaging Earth-like planets with Future Space Observatories," *ApJ* **818**, 163 (Feb. 2016).

[17] Zimmerman, N. T., Eldorado Riggs, A. J., Jeremy Kasdin, N., Carlotti, A., and Vanderbei, R. J., "Shaped pupil Lyot coronagraphs: high-contrast solutions for restricted focal planes," *Journal of Astronomical Telescopes, Instruments, and Systems* **2**, 011012 (Jan. 2016).

[18] Kasdin, N. J., Vanderbei, R. J., Littman, M. G., Carr, M., and N., S. D., "The shaped pupil coronagraph for planet finding coronagraphy: optimization, sensitivity, and laboratory testing," *Proc.SPIE* **5487**, 5487 – 5487 – 10 (2004).

[19] Enya, K., Haze, K., Kotani, T., and Abe, L., "Comparative Study of Manufacturing Techniques for Coronagraphic Binary Pupil Masks: Masks on Substrates and Free-Standing Masks," *PASJj* **64**, 123 (Dec. 2012).

[20] N'Diaye, M., Choquet, E., Egron, S., Pueyo, L., Leboulleux, L., Levecq, O., Perrin, M. D., Elliot, E., Wallace, J. K., Hugot, E., Marcos, M., Ferrari, M., Long, C. A., Anderson, R., DiFelice, A., and Soummer, R., "High-contrast Imager for Complex Aperture Telescopes (HICAT): II. Design overview and first light results," in [*Space Telescopes and Instrumentation 2014: Optical, Infrared, and Millimeter Wave*], *proc. SPIE* **9143**, 914327 (Aug. 2014).

[21] Balasubramanian, K., White, V. E., Yee, K. Y., Echternach, P. M., Muller, R. E., Dickie, M. R., Cady, E. J., Prada, C. M., Ryan, D. J., Poberezhskiy, I., Kern, B. D., Zhou, H., Krist, J. E., Nemati, B., Riggs, A. E., Zimmerman, N. T., and Kasdin, N. J., "Wfirst-afta coronagraph shaped pupil masks: design, fabrication, and characterization," *Journal of Astronomical Telescopes, Instruments, and Systems* **2**, 2 – 2 – 16 (2015).

[22] Zimmerman, N. T., N'Diaye, M., St. Laurent, K. E., Soummer, R., Pueyo, L., Stark, C. C., Sivaramakrishnan, A., Perrin, M., Vanderbei, R. J., Kasdin, N. J., Shaklan, S., and Carlotti, A., "Lyot coronagraph design study for large, segmented space telescope apertures," in [*Space Telescopes and Instrumentation 2016: Optical, Infrared, and Millimeter Wave*], *proc. SPIE* **9904**, 99041Y (July 2016).

[23] Mawet, D., Pueyo, L., Moody, D., Krist, J., and Serabyn, E., "The Vector Vortex Coronagraph: sensitivity to central obscuration, low-order aberrations, chromaticism, and polarization," in [*Society of Photo-Optical Instrumentation Engineers (SPIE) Conference Series*], *Society of Photo-Optical Instrumentation Engineers (SPIE) Conference Series* **7739** (July 2010).

[24] Fogarty, K., Pueyo, L., Mazoyer, J., and N'Diaye, M., "Tip/tilt optimizations for polynomial apodized vortex coronagraphs on obscured telescope pupils," in [*Society of Photo-Optical Instrumentation Engineers (SPIE) Conference Series*], *Society of Photo-Optical Instrumentation Engineers (SPIE) Conference Series* **10400**, 104000T (Sept. 2017).

[25] Mazoyer, J., Pueyo, L., N'Diaye, M., Fogarty, K., Zimmerman, N., Leboulleux, L., St. Laurent, K. E., Soummer, R., Shaklan, S., and Norman, C., "Active Correction of Aperture Discontinuities-Optimized Stroke Minimization. I. A New Adaptive Interaction Matrix Algorithm," *AJ* **155**, 7 (Jan. 2018).

[26] Mazoyer, J., Pueyo, L., N'Diaye, M., Fogarty, K., Zimmerman, N., Soummer, R., Shaklan, S., and Norman, C., "Active Correction of Aperture Discontinuities-Optimized Stroke Minimization. II. Optimization for Future Missions," *AJ* **155**, 8 (Jan. 2018).

[27] N'Diaye, M., Fogarty, K., Soummer, R., Carlotti, A., Kjetil, D., Mazoyer, J., Pueyo, L., Laurent, K. E. S., , and Zimmerman, N., "Apodized Pupil Lyot Coronagraphs with arbitrary aperture telescopes: novel designs using hybrid focal plane masks," *Proc. SPIE* (2018).

[28] Pueyo, L., Zimmerman, N., Bolcar, M., Groff, T., Stark, C., Ruane, G., Jewell, J., Soummer, R., Laurent, K. S., Wang, J., Redding, D., Mazoyer, J., Fogarty, K., Juanola-Parramon, R., Domagal-Goldman, S., Roberge, A., Guyon, O., and Mandell, A., "The luvoir architecture "a" coronagraph instrument," (2017).

[29] Pueyo, L. and Norman, C., "High-contrast Imaging with an Arbitrary Aperture: Active Compensation of Aperture Discontinuities," *ApJ* **769**, 102 (June 2013).

[30] Mazoyer, J., Pueyo, L., Norman, C., N'Diaye, M., Mawet, D., Soummer, R., Perrin, M., Choquet, É., and Carlotti, A., "Active correction of aperture discontinuities (ACAD) for space telescope pupils: a parametic analysis," in [*Techniques and Instrumentation for Detection of Exoplanets VII*], *proc. SPIE* **9605**, 96050M (Sept. 2015).

[31] Laurent, K. S., Fogarty, K., Zimmerman, N. T., N'Diaye, M., Stark, C. C., Mazoyer, J., Sivaramakrishnan, A., Pueyo, L., Shaklan, S., Vanderbei, R., and Soummer, R., "Apodized Pupil Lyot Coronagraphs designs for future segmented space telescopes," *Proc. SPIE* (2018).

[32] Foreman-Mackey, D., Hogg, D. W., Lang, D., and Goodman, J., "emcee: The MCMC Hammer," *PASP* **125**, 306 (Mar. 2013).

[33] Martinez, P., Dorrer, C., Aller Carpentier, E., Kasper, M., Boccaletti, A., Dohlen, K., and Yaitskova, N., "Design, analysis, and testing of a microdot apodizer for the Apodized Pupil Lyot Coronagraph," *A&A* **495**, 363–370 (Feb. 2009).

[34] Martinez, P., Dorrer, C., Kasper, M., Boccaletti, A., and Dohlen, K., "Design, analysis, and testing of a microdot apodizer for the apodized pupil Lyot coronagraph. II. Impact of the dot size," *A&A* **500**, 1281–1285 (June 2009).

[35] Martinez, P., Dorrer, C., Kasper, M., Boccaletti, A., and Dohlen, K., "Design, analysis, and testing of a microdot apodizer for the apodized pupil Lyot coronagraph. III. Application to extremely large telescopes," *A&A* **520**, A110 (Sept. 2010).

[36] Stark, C. C., Roberge, A., Mandell, A., and Robinson, T. D., "Maximizing the ExoEarth Candidate Yield from a Future Direct Imaging Mission," *ApJ* **795**, 122 (Nov. 2014).